Development of Multi-element Monolithic Germanium Detectors for X-ray Detection at Synchrotron Facilities

L. Manzanillas[a,*], S. Aplin[b], A. Balerna[c], P. Bell[d], J. Casas[e], M. Cascella[d], S. Chatterji[f], C. Cohen[g], G. Dennis[f], P. Fajardo[g], H. Graafsma[h], H. Hirsemann[h], F. J. Iguaz[a], K. Klementiev[d], T. Kołodziej[i], T. Martin[g], R. Menk[k], F. Orsini[a], M. Porro[b,l], M. Quispe[e], B. Schmitt[j], N. Tartoni[f], M. Turcato[b], C. Ward[d], E. Welter[h]

[a]*Synchrotron SOLEIL, L'Orme des Merisiers, Départementale 128, Saint-Aubin, 91190, France*
[b]*European XFEL, Holzkoppel 4, Schenefeld, 22869, Germany*
[c] *Laboratori Nazionali di Frascati, Via Enrico Fermi 54 (già 40), Frascati (Roma), 00044, Italy*
[d]*MAX IV Laboratory, Lund University, Fotongatan 2, Lund, 224 84, Sweden*
[e]*ALBA-CELLS Synchrotron Radiation Facility, Carrer de la Llum 2-26, Cerdanyola del Valles, Barcelona, 08290, Spain*
[f]*Diamond Light Source Ltd, Harwell Science and Innovation Campus, Didcot, OX1 10DE, United Kingdom*
[g]*The European Synchrotron Radiation Facility (ESRF), 71 avenue des Martyrs, Grenoble, 38000, France*
[h]*Deutsches Elektronen-Synchrotron DESY, Notkestr. 85, Hamburg, 22607, Germany*
[i]*Jagiellonian University, ul. Golebia 24, Kraków, 31-007, Poland*
[j]*Paul Scherrer Institute, Forschungsstr 111, Villigen PSI, 5232, Switzerland*
[k]*Elettra-Sincrotrone Trieste , S.C.p.A., S.S. 14-km 163.5 in AREA Science Park, Basovizza, Trieste, 34149, Italy*
[l]*Department of Molecular Sciences and Nanosystems, Ca' Foscari University of Venice, Dorsoduro 3246, Venezia, 30172, Italy*

Abstract

In past years efforts have concentrated on the development of arrays of Silicon Drift Detectors for X-ray spectroscopy. This is in stark contrast to the little effort that has been devoted to the improvement of germanium detectors, in particular for synchrotron applications. Germanium detectors have better energy resolution and are more efficient in detecting high energy photons than silicon detectors. In this context, the detector consortium of the European project LEAPS-INNOV has set an ambitious R&D program devoted to the development of a new generation of multi-element monolithic germanium detectors for X-ray detection. In order to improve the performance of the detector under development, simulations of the different detector design options have been performed. In this contribution, the efforts in terms of R&D are outlined with a focus on the modelization of the detector geometry and first performance results. These performance results show that a signal-to-background ratio larger than 1000 can be achieved in the energy range of interest from 5 keV to 100 keV.

Keywords: Germanium detectors, Semiconductors, Synchrotrons

1. Introduction

X-rays Absorption Fine Structure (XAFS) has been widely used in experiments at synchrotron facilities in order to determine the electronic and geometrical structure in a sample

*Corresponding author
Email address: luis.manzanillas@synchrotron-soleil.fr (L. Manzanillas)

in a variety of scientific fields, including biology, environmental science, catalysts research, and material science [1]. XAFS and similar techniques require energy resolving photon-counting detectors capable of coping with a high count rate. The ongoing XAFS experiments at synchrotron facilities are limited by the performance of the current generation of Silicon (Si) and Germanium (Ge) detectors [2]. While efforts have concentrated to the development of arrays of Silicon Drift Detectors (SDDs), little effort has been devoted to the improvement of Hyper-Pure Germanium (HPGe) detectors for synchrotron applications. HPGe detectors provide better energy resolution and detection efficiency for high energy photons than SDDs. The detector consortium of the European project LEAPS-INNOV [3, 4] has set an ambitious R&D program devoted to the development of a new generation of multi-element monolithic HPGe detectors for X-ray detection. This new generation of HPGe detectors will be able to cope with a high throughput in a broad energy range, from 5 keV to 100 keV. Accepting and processing a high count rate without degradation of the energy resolution is crucial for the success of this new new generation of HPGe detectors. Therefore, new electronics are being also developed as part of the project. This new electronics will be able to process count rates ranging from 20 kcps/mm^2 up to 250 kcps/mm^2, keeping an excellent energy resolution and minimizing dead time.

HPGe detectors are built as single contact or segmented detectors. While in single contact detectors the noise decreases because there is no capacitance coupling with other neighboring contacts, it limits the count rate that the detector can accept without pile-up. In contrast, in segmented HPGe detectors a considerable increase of count rate maintaining a tolerable pile-up probability can be achieved. Thus, the strategy of the consortium is to develop segmented HPGe detectors. The detectors will be fabricated from crystals with geometry and dimensions as shown in Figure 1. The segmentation of the readout contacts consists of a central hexagonal shape surrounded by six trapezoids and three outer segments. The inter-pixel regions are 100 μm wide. Moreover, a guard ring surrounds the readout contacts. The detectors will be made of n-type Ge crystals, with an expected net impurity concentration of the order of $\sim 10^{10}$ /cm^3.

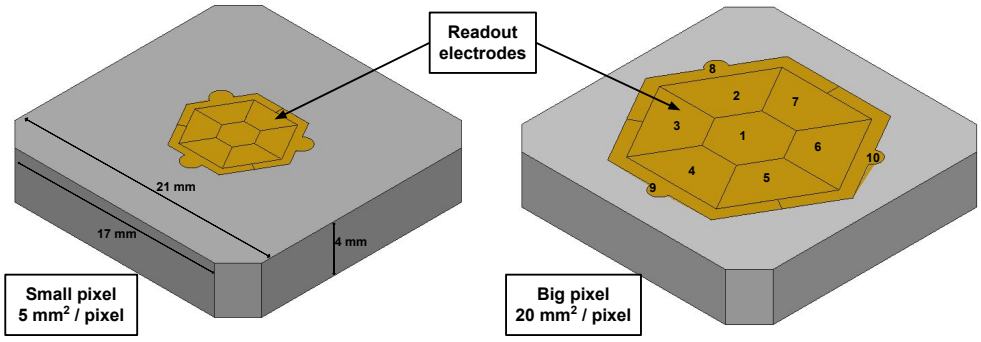

Figure 1: Geometry of HPGe detector prototypes being developed by the LEAPS-INNOV detector consortium. The detector overall dimensions are 21 mm $\times$ 21 mm $\times$ 4 mm (thickness). The bottom of the detectors (n+) facing the X-rays is non segmented and it is used to place the high voltage connection. The top of the detectors (p+) is segmented into 10 pixels and it is used to readout the signals in hole collection mode. Two pixel sizes are being developed, small pixel (SP) of 5 mm^2 shown on the left side and big pixel (BP) of 20 mm^2 shown on the right side.

Aiming to study, characterize and optimize the performance of the HPGe detectors under development, detailed multi-physics simulations were performed and are described in next section.

2. Simulation chain

In most of XAFS experiments, only the energies deposited in the detectors are recorded. However, the time development of the charges induced in the read out electrodes i.e. the pulses, are used to optimize the acquisition parameters to maximize the detector performance. In addition, pulse shape analysis can be used to improve the position reconstruction and background rejection efficiency. In particular, the rejection of events with energy deposition being detected in several electrodes, i.e. multi-site events, is vital to decrease the background and to improve the energy resolution.

A precise simulation of the detector pulses is essential to develop and optimize the required algorithms for signal selection and energy reconstruction. To this end, a complete simulation chain, including all the steps from the interaction of X-rays with the HPGe detector and its environment to a reconstructed energy spectrum using simulated data-like raw waveforms was developed. Figure 2 shows the flowchart of the simulation chain. The required information about the HPGe detector such as the detector geometry, impurity density, bias voltage, among others, are used to calculate the detector fields. Once all the information about the fields has been completed, the information about the interaction of the X-rays with the detector is used to simulate perfect pulses. The interaction of the X-rays with the HPGe detector and its environment is performed using the Geant4 simulation toolkit [5]. Finally, the signal amplification and electronics noise are included and a data-like waveform is produced for each event.

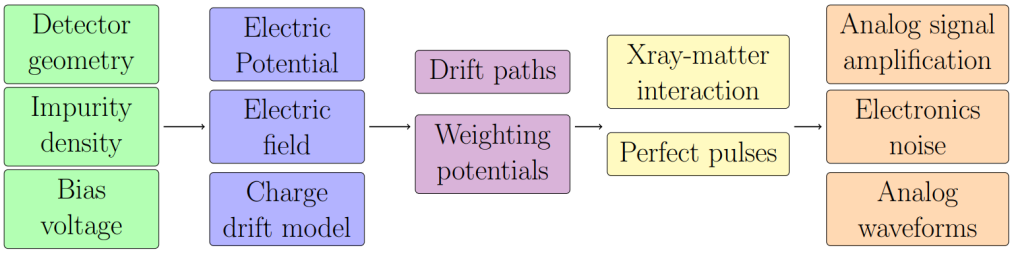

Figure 2: Flowchart of the simulation chain.

2.1. Simulation of detector fields

The shape of the pulses of the signals in HPGe detectors is mainly governed by the fields in the detector. These fields are dependent on the detector and electrodes geometry, bias voltage and impurity profile. To simulate the detector fields, a bias voltage of 200 V and an impurity density of the order of 10^{10} /cm^3 ($\sim$ constant) in the bulk material was used. A precise calculation of all the detector fields is crucial to a faithful reproduction of the detector signals. To this end, the SolidStateDetectors.jl (SSD) [6] and COMSOL-Multiphysics [7] packages were used to calculate the detector fields. These packages allow one to calculate the electric potential, electric field and weighting potentials in the whole detector volume. In addition, SSD also allows one to simulate the drifts of charge carriers in solid state detectors together with the corresponding pulses. Moreover, SSD has been optimized for large HPGe detectors, and has been developed as an open software package using the julia programming language [8] to facilitate the integration of additional developments. Thus, the full simulation chain was developed using SSD and julia.

To compute the electric potential and the electric field, Poisson's equation must be solved

$$\nabla(\epsilon_r(\vec{r})\nabla\Phi(\vec{r})) = -\frac{\rho(\vec{r})}{\epsilon_0} \tag{1}$$

with $\Phi(\vec{r})$ being the electric potential, ρ the charge density, ϵ_r the dielectric distribution, and ϵ_0 the vacuum dielectric constant. In SSD, the electric potential is calculated through the successive over relaxation (SOR) method. Equation 1 is numerically solved on a three-dimensional adaptive grid. The adaptive grid allows for multithreading and saves computation time since it only increases the grid point density in areas where it is critical. The electric field is calculated from the electric potential $\Phi(\vec{r})$. The field vector components on each grid point are the means of the electric field in each direction calculated as finite differences.

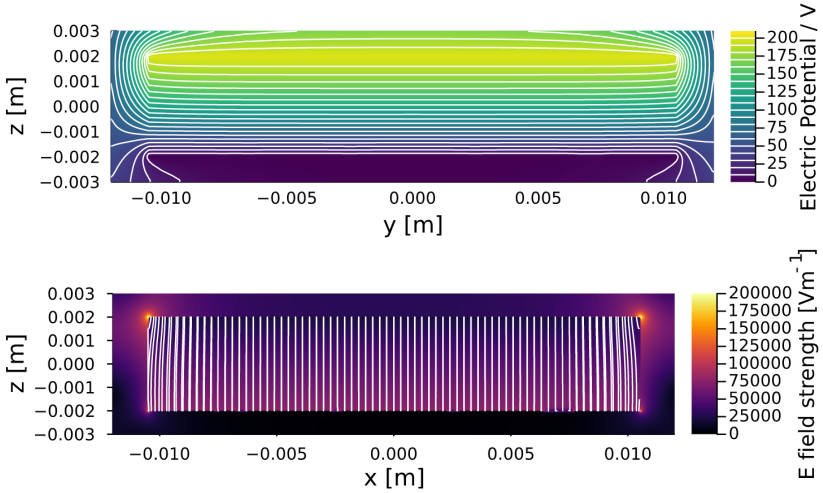

Figure 3: Top: Electric potential in the HPGe detector with big pixel geometry configuration, calculated with the SSD package and assuming a bias voltage of 200 V. Bottom: Electric field strength and electric field lines.

Figure 3 shows the electric potential (Top) and the electric field lines (Bottom) that have been calculated with SSD assuming a bias voltage of 200 V. The Ge sensor is fully depleted, and in almost the whole detector the charge carriers will drift vertically in direction of the electrodes.

2.2. Simulation of detector pulses

In HPGe detectors the electric signals corresponds to the sum of the charges induced on the electrodes of the detector by drifting electrons and holes. In SSD, the Shockley-Ramo theorem is used to calculate the time development of the induced charge in each electrode. The charge carriers will be seen and collected by a given electrode as a function of its position and the weighting potential of the electrode. The weighting potential is a theoretical potential that describes what fraction of a charge at position $\vec{r}$ is seen by a contact C_i. The weighting potential can take values between 0, i.e. the charge is not seen by the electrode, and 1, i.e. the charge is seen and collected by the electrode. The weighting potential is calculated solving Laplace equation

$$\nabla(\epsilon_r(\vec{r})\nabla\Phi_i^w(\vec{r})) = 0 \tag{2}$$

where $\Phi_i^w(\vec{r})$ is the electric potential and $\epsilon_r(\vec{r})$ is the dielectric distribution. To calculate the weighting potential of a given contact, a voltage of 1 V is applied to that contact and 0 V to all other contacts. Figure 4 shows the calculated weighting potential for the central contact with hexagonal shape of the BP detector geometry configuration.

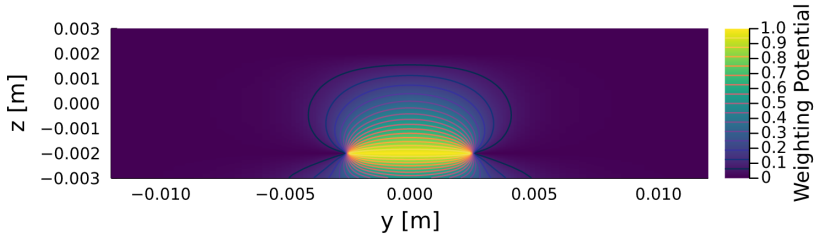

Figure 4: Weighting potential of the hexagonal shape central electrode of the big pixel (BP) geometry configuration.

The drift velocity vectors are calculated separately for electrons and holes for each grid point using the calculated electric field and the respective electron or hole drift velocity model. The default drift velocity model implemented in SSD uses measured parameters for HPGe at 77 K [9]. Using these parameters the charge carriers are drifted and noiseless pulses are generated in each readout contact. The final steps in the simulation of the pulses include the signal amplification and electronics noise. The former is accounted for by convolving the perfect pulses with a simulated transfer function. The electronics noise is included adding baseline data from a commercial HPGe detector to the amplified pulses. These preliminary transfer function and electronics noise will be adjusted with the final measured parameters once the detectors are available.

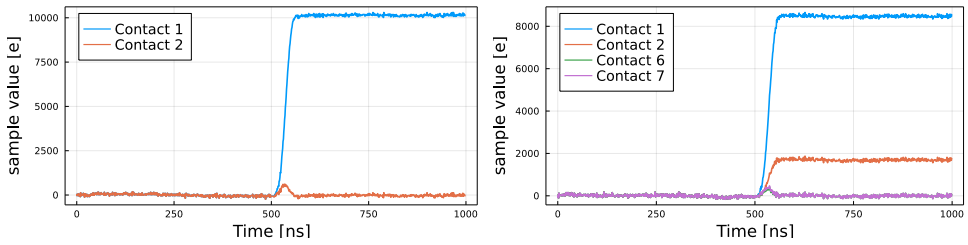

Figure 5: Left: Example of simulated waveforms for an event collected in a single contact. Right: Example of simulated waveforms for an event showing charge sharing being collected in two contacts. The small "bump" without net transfer of charge observed in neighboring channels is the result of the mutual capacitance coupling between contacts.

Figure 5 shows simulated waveforms containing pulses with all the steps of the simulation chain for an event collected in a single contact (Left) and a charge sharing event collected in two contacts (Right). A small bump is also induced in the neighboring contacts without net transfer of charge. This "bump" induced in neighboring channels is the result of the mutual capacitance coupling between neighboring contacts. A total capacitance for each contact of around 1 pF and 3 pF was estimated with SSD for the SP and BP configurations respectively.

3. Detector performance

To estimate the detector performance, an X-ray beam was incident on the detector with energies ranging from 5 keV to 100 keV. For each energy, about 2 M of events were simulated. For every event the complete simulation chain was applied and the corresponding data-like raw waveforms of all readout contacts were generated. The energy of each event was estimated by applying a trapezoidal filter to the data-like raw waveform of the contact with the highest collected charge. This trapezoidal filter is expected to be implemented in the Digital Pulse Processor (DPP). The final energy spectrum obtained in this way with all the reconstructed events was used to define a region of interest (RoI) and a background region (BR). The RoI was defined with a band around the energy of the beam ($E \pm 0.5$ keV), while the background region was taken from an equivalent band with the same width shifted 3.5 keV to lower energies. The signal efficiency and background level were defined as the number of events in the RoI or BR over the total number of events in the spectrum. The potential of using a DPP capable of performing an online selection of the events was also studied. This DPP selection consisted in identifying and removing charge sharing events using an energy threshold of 1 keV. Charge sharing events deteriorate the energy resolution and populate the background region.

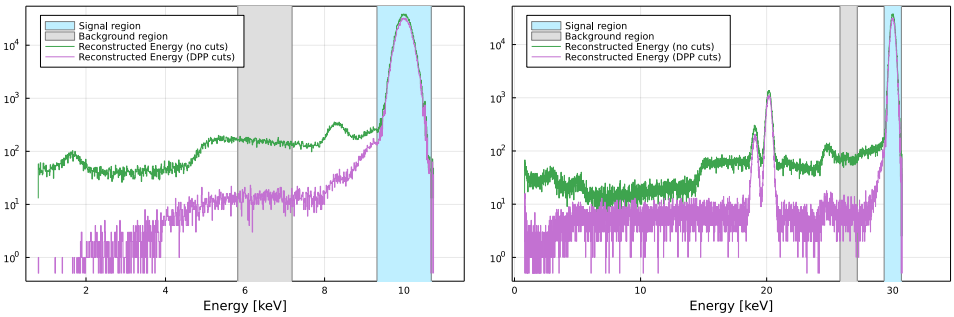

Figure 6: Left: Reconstructed energy spectrum for an incident X-ray beam of 10 keV. Right: Reconstructed energy spectrum for an incident X-ray beam of 30 keV. Two peaks around 20 keV are also observed and have their origin in the escape peaks of Ge fluorescence.

Figure 6 shows two examples of reconstructed energy spectra for incident X-ray beams of 10 keV and 30 keV with (violet) and without (green) a DPP selection. The RoI and BR are shown with a blue and with a grey band respectively. The main peak in the spectra corresponds to the energy of the beams. Above 10 keV two other peaks are also present as can be seen in Figure 6 (Right). These two peaks correspond to the Ge fluorescence escape peaks at 9.86 keV and 10.98 keV. From the energy spectra shown in Figure 6, the detector performance can be extracted. The estimated signal efficiency in the region of interest is shown Figure 7 (Left). The lower values are obtained for the small pixel detector configuration. Values close to 100% are obtained for energies below 11 keV were most of the photons are completely absorbed by photoelectric effect and the corresponding electrons are absorbed in a small volume of the detector ($<1\text{mm}^3$). A decrease of the signal efficiency is observed between 11 keV and 20 keV because of Ge fluorescence. The photons from Ge fluorescence, escape the detector, decreasing the number of events in the main peak.

The simulations also showed that the efficiency can be improved by using either a collimator, or a specific selection with a DPP, or both to remove charge sharing events. In this simulations,

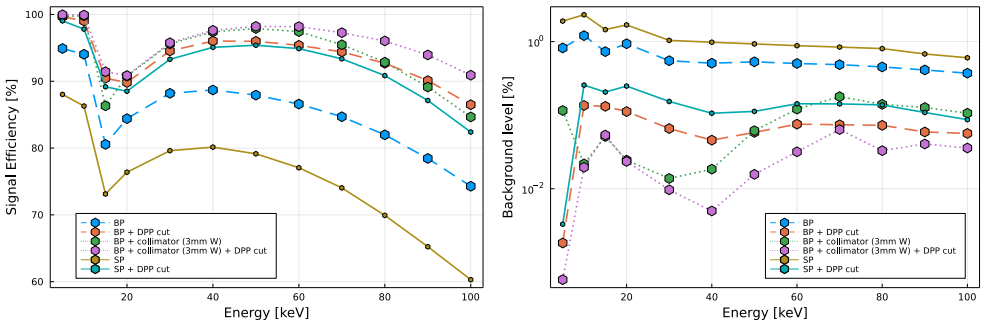

Figure 7: Left: Estimated signal efficiency for the SP and BP configuration with and without a DPP selection, and BP plus a collimator with and without a DPP selection. Right: Estimated background level using the same configuration as the left plot.

the collimator consists in a cylinder of tungsten, with a thickness of 3 mm covering the whole surface of the HPGe detector and containing holes corresponding to the pixel geometry as shown in Figure 8 (Left). By using a collimator, 600 μm wide regions around the inter-pixel regions where most of the charge sharing events take place are shielded. Given the small area of the small pixel (SP) configuration, the collimator was considered only for the BP configuration.

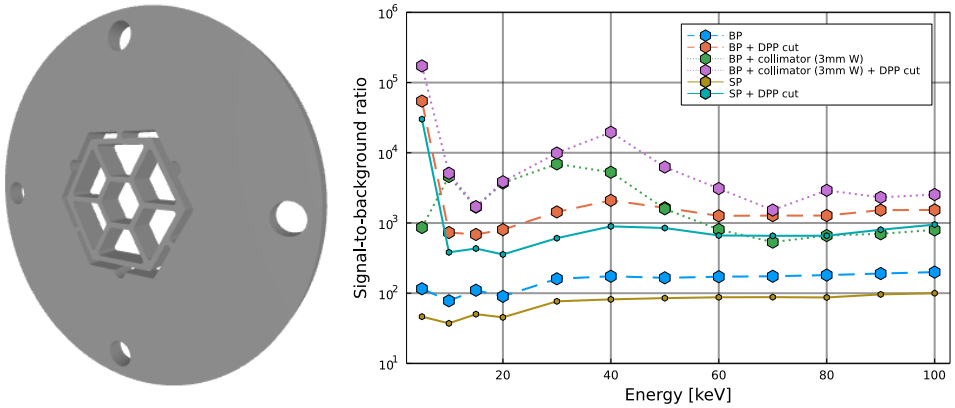

Figure 8: Left: Geometry of collimator being studied. It consist of cylinder of tungsten covering the regions between the pixels. Right: Signal to background ratio in the region of interest for all the configurations studied.

Figure 7 (Right) shows the estimated background level. The lowest background level is achieved for the BP configuration in conjunction with a collimator plus a specific DPP selection. This combination allows one to remove most of the events populating the background region. Finally, to evaluate the combined effect of signal efficiency and background level, a signal-to-background ratio (S/B) parameter was defined. This parameter was evaluated as the coefficient between the signal efficiency and the background level. Figure 8 (Right) shows the expected S/B for the different configurations under investigation. The target of the project is to achieve a S/B ratio larger than 1000 for energies below 10 keV, which is the level that can be achieved with current commercial detectors. From the different configurations analyzed, the best performance

is obtained for the BP configuration combining a 3 mm tungsten collimator and a DPP selection. In this configuration a S/B ratio larger than 1000 in the whole energy range is reached. The achieved values at 40 keV for different configurations are reported in Table 1.

Configuration	Signal Efficiency [%]	Background level [%]	S/B
SP	80.1	0.9	81.7
SP + DPP	95.1	0.1	895.1
BP	88.7	0.5	174.3
BP + DPP	96.1	0.05	2099.1
BP + DPP + collimator	97.6	0.005	19593.7

Table 1: Estimated values of signal efficiency, background level and S/B at 40 keV

4. Conclusions

The LEAPS-INNOV detector consortium has set an ambitious R&D program launched in April 2021 for the development of a new generation of monolithic pixelized HPGe detectors for synchrotron applications. A full simulation chain based on the SSD package and julia has been developed to study and optimize the performance of the detectors under development. First results suggest that both, signal efficiency and background level, can be improved, allowing to achieve a S/B larger than 1000 in most of the configurations investigated. These results are compatible with the requirements of the project. The best performance could be obtained combining a specific selection with a DPP and a collimator in order to remove charge sharing events. This combination allows to reach a S/B > 1000 in the whole energy range. The simulation chain will be optimized once the detectors are available for data taking.

5. Acknowledgments

This project has received funding from the European Union's Horizon 2020 research and innovation programme under grant agreement No 101004728.

References

[1] G. Bunker, "Introduction to XAFS: A Practical Guide to X-Ray Absorption Fine Structure Spectroscopy". Cambridge, U.K.: Cambridge, U.K.: Cambridge Univ. Press, 2010.
[2] N. Tartoni, et al., "Hexagonal Pad Multichannel Ge X-Ray Spectroscopy Detector Demonstrator: Comprehensive Characterization," in IEEE Transactions on Nuclear Science, vol. 67, no. 8, pp. 1952-1961, Aug. 2020.
[3] LEAPS pilot to foster open innovation for accelerator-based light sources in Europe, European Union's Horizon 2020, Grant Agreement No 101004728.
[4] F. Orsini, et al., "XAFS-DET: a new high throughout X-ray spectroscopy detector system developed for synchrotron applications", August 2022 NDIP2020 Conference, this record.
[5] S. Agostinelli *et al.* [GEANT4], "GEANT4–a simulation toolkit," Nucl. Instrum. Meth. A **506** (2003), 250-303 doi:10.1016/S0168-9002(03)01368-8
[6] I. Abt, et al., "Simulation of semiconductor detectors in 3D with SolidStateDetectors.jl," JINST **16** (2021) no.08, P08007 doi:10.1088/1748-0221/16/08/P08007 [arXiv:2104.00109].
[7] COMSOL Multiphysics® v.6.0. www.comsol.com. COMSOL AB, Stockholm, Sweden.
[8] Bezanson, J. et al., 2012. Julia: A fast dynamic language for technical computing. [arXiv:1209.5145].
[9] B. Bruyneel, P. Reiter and G. Pascovici, "Characterization of large volume HPGe detectors. Part I: Electron and hole mobility parameterization," Nuclear Instruments and Methods in Physics Research Section A: Accelerators, Spectrometers, Detectors and Associated Equipment. Volume 569, Issue 3, 21 December 2006.